

Product of Gaussian Mixture Diffusion Model for non-linear MRI Inversion

Laurenz Nagler¹, Martin Zach²^[0000-0003-1941-875X], and Thomas Pock¹^[0000-0001-6120-1058]

¹ Technical University of Graz, 8010 Graz, Austria

lnagler@student.tugraz.at, thomas.pock@icg.tugraz.at

² École polytechnique fédérale de Lausanne, 1015 Lausanne, Switzerland
martin.zach@epfl.ch

Abstract. Diffusion models have recently shown remarkable results in magnetic resonance imaging reconstruction. However, the employed networks typically are black-box estimators of the (smoothed) prior score with tens of millions of parameters, restricting interpretability and increasing reconstruction time. Furthermore, parallel imaging reconstruction algorithms either rely on off-line coil sensitivity estimation, which is prone to misalignment and restricting sampling trajectories, or perform per-coil reconstruction, making the computational cost proportional to the number of coils. To overcome this, we jointly reconstruct the image and the coil sensitivities using the lightweight, parameter-efficient, and interpretable product of Gaussian mixture diffusion model as an image prior and a classical smoothness priors on the coil sensitivities. The proposed method delivers promising results while allowing for fast inference and demonstrating robustness to contrast out-of-distribution data and sampling trajectories, comparable to classical variational penalties such as total variation. Finally, the probabilistic formulation allows the calculation of the posterior expectation and pixel-wise variance.

Keywords: Diffusion Model · MRI Reconstruction · Non-linear Inverse Problem.

1 Introduction

Magnetic resonance imaging (MRI) is one of the pillars of modern medicine, exhibiting high spatial resolution and contrast flexibility. However, these strengths are limited by low temporal resolution, long scan times and artefacts induced by patient movement.

This can be overcome by acquiring less data, resulting in an ill-posed reconstruction problem. One way to obtain solutions to the problem is parallel imaging (PI), where multiple spatially structured receiver coils are used. The individual coil data is then combined in either the image domain [20] or the frequency domain [10]. Another way of tackling this problem is through variational

methods or compressed sensing (CS) theory, which leverages sparse representations of the data in a specific domain and incoherent sampling to enable image reconstruction [1, 17].

In recent years, data-driven methods have achieved remarkable results in MRI image reconstruction [7, 13, 30]. These models can be categorized by whether they follow a Bayesian separation of likelihood and prior, i.e. whether the learned components account for the measurement setup or not. In the context of MRI, the Bayesian separation obviates the need for multi-coil data for learning [30] and enables the learned model to be used for reconstructing images from arbitrary k-space sampling trajectories. Methods pursuing this Bayesian separation in MRI include works based on generative adversarial networks (GANs) [18], energy based models (EBMs) [30], and, more recently, diffusion models [7, 13, 16, 24]. Diffusion models deliver state-of-the-art results but have shortcomings: The networks are, in general, not the gradient of a potential [22], and the time conditioning is opaque, seemingly unrelated to the underlying stochastic differential equation. Furthermore, models with millions of parameters are often accompanied by long inference times, a lack of interpretability and the need for heuristics to be applied to data of arbitrary size [7, 9]. Existing methods for PI such as [13, 16] typically require off-line coil sensitivity estimation, e.g. with ESPiRiT [28]. This is sensitive to patient motion and hard to adapt to arbitrary k-space sampling trajectories [14]. In a different line of work, [7] overcomes this by reconstructing individual coil images, making the computational cost proportional to the number of coils, which is unacceptably large when paired with the typical large networks used to model the score. In [4], the authors propose to tackle blind inverse problems by additionally learning a diffusion model on the parameters of the forward operator. In the context of PI, this translates to learning a diffusion model on the coil sensitivities, again making the computational cost proportional to the number of coils and introducing the engineering challenge of training and tuning the additional diffusion model. In [11], the authors propose an algorithm for PI, where the coil sensitivities are assumed to be sufficiently close to an initial guess, again requiring off-line estimation.

Recently, Zach et al. [31] introduced the product of Gaussian mixture diffusion model (PoGMDM),

$$p_{\theta}(x, t) \propto \prod_{i,j=1}^{n,m} \prod_{k=1}^o \psi_k((K_k x)_{i,j}, w_k, t), \quad (1)$$

a diffusion model with fields-of-experts-type structure and relations to classical shrinkage-type regularization. Here, to model the density of $n \times m$ images, for all $k = 1, \dots, o$,

$$\psi_k(x, w, t) = \sum_{i=1}^L w_i / \sqrt{2\pi\sigma(t)^2} \exp((x - \mu_i)^2 / (2\sigma_k^2(t))) \quad (2)$$

is a Gaussian mixture model (GMM) with weights w_k , $K_k : \mathbb{R}^{n \times m} \rightarrow \mathbb{R}^{n \times m}$ is a convolution operator, and the time conditioning adapts the variance σ_k^2 in the

GMM in accordance with the stochastic differential equation (SDE) based on characteristics of K_k . This model is analytically tractable and interpretable, has few learnable parameters and allows for fast inference. In their work, they only considered denoising due to the close relations between generative modelling and denoising via Tweedies identity. In this work, we demonstrate the feasibility of PoGMDM as an image prior in joint non-linear MRI reconstruction by pairing it with simple smoothness priors on the coil sensitivities.

2 Background

2.1 Generative Modeling and Diffusion

In generative modeling, we are interested in learning a parametric model approximating a reference distribution from a given dataset. Let X be the random variable of the reference distribution with associated density p_X . Learning a model p_θ approximating p_X is hard as the high dimensional density space is sparsely populated. One way to ease learning is to smooth (thus filling low-density regions) and approximate the density at different scales [23].

Song et al. generalized this idea to SDEs [25]. In this work, we consider the SDE

$$dY_t = \sqrt{2}dw_t, \quad Y_0 = X \quad (3)$$

where w is the standard Wiener process and is a random variable Y_t with density $p_Y(\cdot, t)$.

The Fokker-Planck equation [21] links Y_t to its density, which is given as the partial differential equation (PDE) $\partial p_Y(\cdot, t)/\partial t = \Delta p_Y(\cdot, t)$ with $p_Y(\cdot, 0) = p_X$. This is the classic heat diffusion with the solution $p_Y(\cdot, t) = \mathcal{N}(0, 2tI) * p_X$, thus constructing a scale space in the space of probability [31]. In practice, a model $p_\theta(\cdot, t) \approx p_Y(\cdot, t)$ can be learned by optimizing the objective function

$$\min_{\theta} \int_0^{\infty} \mathbb{E}_{(x, y_t) \sim p_{X, Y_t}} [\|x - y_t - 2t\nabla p_\theta(y_t, t)\|_2^2] dt \quad (4)$$

known as denoising score matching [25, 29]. With this configuration, sampling amounts to running the diffusion process,

$$d\bar{Y}_t = -2\nabla \log p_Y(\bar{Y}_t, t)dt + \sqrt{2}d\bar{w}_t, \quad \bar{Y}_T = Y_T, \quad (5)$$

where dt is a negative infinitesimal time step and \bar{w} is the reverse time Wiener process starting, from a time T to zero. The only unknown quantity in (5) is the gradient of the log density p_Y (score) at each time t , that we model with $p_\theta(\cdot, t)$.

2.2 Inverse Problems and Diffusion Priors

Solving an inverse problem amounts to recovering an unknown signal x from a set of measurements $z = \mathcal{A}(x) + \epsilon$, where \mathcal{A} models the acquisition and ϵ summarizes measurement noise. The probabilistic treatment of the recovery problem amounts

to constructing a posterior density $p_{X|Z}(\cdot, z)$ from the likelihood $p_{Z|X}$, which makes use of the known acquisition physics encoded in \mathcal{A} , and prior information about the reconstruction, encoded in p_X ; see [8] for more details. The diffusion framework can account for this by conditioning the stochastic process (5) on the measurements, resulting in

$$d\bar{Y}_t = -2\nabla \log p_{Y|Z}(\bar{Y}_t, z, t)dt + \sqrt{2}d\bar{w}_t, \quad \bar{Y}_T = Y_T, \quad (6)$$

where $\log p_{Y|Z}(y_t, z, t) \propto \log p_{Z|Y}(y_t, z, t) + \log p_Y(y_t, t)$. The relationship between Y_t and Z is usually only known at $t = 0$, necessitating approximations for $t > 0$ [5, 13, 24].

3 Methods

The conditional reverse SDE (6) is valid for general, linear and nonlinear, inverse problems. In this section, we state our acquisition model for PI MRI and formulate our approximations. The resulting reconstruction algorithm is summarized in Algorithm 1.

3.1 Image Reconstruction Algorithm

We view the PI recovery problem as a non-linear inverse problem of jointly reconstructing the spin density $x \in \mathbb{C}^{n \times m}$ as well as the coil sensitivities $\sigma = (\sigma_1, \dots, \sigma_c) \in \mathbb{C}^{n \times m \times c}$ from measured data $z = (z_1, \dots, z_c) \in \mathbb{C}^{f \times c}$ where $f \in \mathbb{N}$ is the number of measured spatial frequencies. The relation between the data and the variables is given as

$$z = \mathcal{A}(x, \sigma) + \epsilon = \begin{pmatrix} MF(\sigma_1 \odot x) \\ \vdots \\ MF(\sigma_c \odot x) \end{pmatrix} + \epsilon \quad (7)$$

where $M : \mathbb{C}^{n \times m} \rightarrow \mathbb{C}^f$ is a binary sampling operator, $F : \mathbb{C}^{n \times m} \rightarrow \mathbb{C}^{n \times m}$ is the discrete Fourier transform and $\epsilon \in \mathbb{C}^{f \times c}$ is additive Gaussian noise. Recovering (x, σ) from z is hard even in the fully sampled case [27]. To approach this, we introduce priors on the spin density and the sensitivities: Motivated by the bilinear form of (7), we view the recovery problem as a blind inverse problem [4, 11] and utilize the approximation

$$p_{X, \Sigma|Z}(x_t, \sigma_t, z, t) \propto p_{Z|X, \Sigma}(x_t, \sigma_t, z, t) \cdot p_\theta(x_t, t) \cdot p_\Sigma(\sigma_t, t). \quad (8)$$

i.e. that the distribution of (X, Σ) factorizes. We choose a Gaussian likelihood of the form $p_{Z|X, \Sigma}(x_t, \sigma_t, z, t) \propto \exp(-\frac{1}{2}\|\mathcal{A}(x_t, \sigma_t) - z\|_2^2)$. This is a popular and simple choice originating from [13], but only correct for $t = 0$ in the diffusion process [7]. $p_\theta(\cdot, t)$ is the PoGMMDM (1) trained on reference images, see the

details in section 3.2. Following [30] we chose, the classical smoothness prior $p_{\Sigma}(\sigma, 0) \propto \exp(-s(\sigma))$, with

$$s : \mathbb{C}^{n \times m \times c} \rightarrow \mathbb{R} : \sigma \mapsto \frac{1}{2} \sum_{i=1}^c (\|D_{\text{D}} \text{Re}(\sigma_i)\|_2^2 + \|D_{\text{D}} \text{Im}(\sigma_i)\|_2^2), \quad (9)$$

where $D_{\text{D}} : \mathbb{R}^{n \times m} \rightarrow \mathbb{R}^{n \times m \times 2}$ is a forward finite differences operator with Dirichlet boundary conditions. We use an adapted version of the algorithm proposed in [9] for posterior sampling. The likelihood is incorporated by doing a gradient descent step in each iteration, where the gradient of the log-likelihood w.r.t. x_t is

$$\nabla_{x_t} \log p_{Z|X, \Sigma}(x_t, \sigma_t, y, t) = \sum_{i=1}^c \bar{\sigma}_{t,i} \odot (F^* M^* (MF(\sigma_{t,i} \odot x_t) - z_i)), \quad (10)$$

with $\bar{\sigma}_{t,i}$ being the complex conjugate sensitivity of the coil indexed by i . We found it sufficient to fix $p_{\Sigma}(\cdot, t) = p_{\Sigma}(\cdot, 0)$ for all $t > 0$, thus depart from the diffusion framework and perform proximal gradient descent steps on σ_t . The proximal map of $\log p_{\Sigma}$ has a closed-form solution

$$\text{prox}_{\mu s}(\sigma) = \begin{pmatrix} Q_{\mu}(\text{Re}(\sigma_1)) + iQ_{\mu}(\text{Im}(\sigma_1)) \\ \vdots \\ Q_{\mu}(\text{Re}(\sigma_c)) + iQ_{\mu}(\text{Im}(\sigma_c)) \end{pmatrix}, \quad (11)$$

with $\mu \in \mathbb{R}_{>0}$ and $Q_{\mu} : \mathbb{R}^{n \times m} \rightarrow \mathbb{R}^{n \times m}; x \mapsto \mathcal{S}^* (\mathcal{S}(\mu x) \odot (\tau + \mu)^{-1})$. Here, \mathcal{S} is the two-dimensional discrete sine transform, and τ are the eigenvalues of the two-dimensional discrete Laplace operator [30]. The gradient of the log-likelihood w.r.t. σ_t is

$$\nabla_{\sigma_t} \log p_{Z|X, \Sigma}(x_t, \sigma_t, y, t) = \begin{pmatrix} x_t \odot (F^* M^* (MF(\sigma_{t,1} \odot x_t) - z_1)) \\ \vdots \\ x_t \odot (F^* M^* (MF(\sigma_{t,c} \odot x_t) - z_c)) \end{pmatrix}. \quad (12)$$

Similar to [7], we apply the prior, trained on magnitude images, to the real- and imaginary parts individually. We summarize the joint reconstruction in Algorithm 1, where ξ stores independent samples of a standard complex-normal distribution.

3.2 Model Architecture and Implementational Details

We largely use the same model parameterization as in [31]: The convolution operators $\{K_k = \gamma_k \tilde{K}_k\}_{k=1}^o$ are nonseparable shearlets \tilde{K}_k comprising two scales with five shearings for each of the two (horizontal and vertical) cones, yielding $o = 20$, each endowed with a learnable weight $\gamma_k \geq 0$. Following [2, 31], we learn the construction blocks of the shearlet system, a one-dimensional low-pass-filter $h \in \mathbb{R}^9$ and a two-dimensional directional high-pass filter $P \in \mathbb{R}^{17 \times 17}$. For each

Algorithm 1: Joint Reconstruction Algorithm

Output: x^0, σ^0

- 1 $x^N \sim \mathcal{N}(0, \zeta_{max}^2 I)$
- 2 **for** $i \in [N - 1, 0]$ **do**
- 3 **for** $k \in [\text{Re}, \text{Im}]$ **do**
- 4 $x^{k,i} = x^{k,i+1} + (\zeta_{i+1}^2 - \zeta_i^2) \nabla \log p_\theta(x^{k,i+1}, \zeta_{i+1}^2) + \sqrt{\zeta_{i+1}^2 - \zeta_i^2} \xi_i^k$
- 5 $x^i = x^{\text{Re},i} + ix^{\text{Im},i}$
- 6 $x^i = x^i + \lambda \nabla_{x^i} \log p_{Z|X,\Sigma}(x^i, \sigma^{i+1}, z, t)$
- 7 **for** $j \in [0, M - 1]$ **do**
- 8 **for** $k \in [\text{Re}, \text{Im}]$ **do**
- 9 $x^{k,i} = x^{k,i} + \epsilon_i \nabla \log p_\theta(x^{k,i}, \zeta_i^2) + \sqrt{2\epsilon_i} \xi_j^k$
- 10 $x^i = x^{\text{Re},i} + ix^{\text{Im},i}$
- 11 $x^i = x^i + \lambda \nabla_{x^i} \log p_{Z|X,\Sigma}(x^i, \sigma^{i+1}, z, t)$
- 12 $\sigma^i = \text{prox}_{\mu s}(\sigma^{i+1} - \mu \nabla_{\sigma^{i+1}} \log p_{Z|X,\Sigma}(x^i, \sigma^{i+1}, z))$

$k = 1, \dots, o$, we chose $\psi_k : \mathbb{R} \times \Delta^L \times \mathbb{R}_{\geq 0} \rightarrow \mathbb{R}_{\geq 0}$ as an $L = 125$ component GMM whose weights w_k are constrained to the L -dimensional unit simplex Δ^L . This results in $9 + 17^2 + o\lceil L/2 \rceil + o = 1578$ (as in [31] the number of learnable weights is half the number of components due to symmetry) learnable parameters that are optimized for (4) with projected AdaBelief [34] for 100 000 steps, where we implement the same constraints as in [31]. Furthermore, we use exponential moving average (EMA), with a momentum of 0.999.

For posterior sampling we choose $N = 1000$, $M = 1$, $\lambda = 1$, $\mu = 10$ and the noise schedule $\zeta(t) = \zeta_{\min}(\zeta_{\max}/\zeta_{\min})^t$ with $\zeta_{\min} = 0.01$ and $\zeta_{\max} = 10$. We calculate ϵ_i according to [25]. Furthermore, we find optimal hyperparameters for each sampling pattern with grid search. The coil sensitivities σ are initialized with the zero-filled coil images normalized by the initial root sum of squares (RSS) reconstruction. Finally, we accelerate sampling by using the algorithm proposed in [6] with vanilla initialization.

3.3 Experimental Data

We use the fastMRI knee dataset [15] for model training, hyper-parameter search, and evaluation. We use the central eleven slices of each scan in the coronal proton density (CORPD) training split, resulting in 5324 images of size 320×320 . For the hyper-parameter search and testing, we divide the validation split into 30 validation files and 58 test files, excluding k-space data with width different from 368 and 372 for simplicity of implementation, again taking the central eleven slices. For out of distribution (OOD) experiments we use the coronal proton density fat suppressed (CORPDFS) validation dataset, again excluding based on the width and using the eleven central slices. Training images are normalized to a maximum of 1 via $x \mapsto x/\|x\|_\infty$.

3.4 Comparison and Evaluation

Our evaluation is twofold: Firstly, we conduct a synthetic single coil experiment, where we retrospectively sample the k-space data of CORPD reference RSS images $x \in \mathbb{R}^{320 \times 320}$. Secondly, a PI experiments with joint reconstruction on the CORPD/FS datasets. In both experiments, we compare against the Charbonnier smoothed isotropic total variation (TV) as a classical variational penalty in the joint nonlinear inversion algorithm proposed in [30]. ScoreMRI [7] (single coil), the fastMRI baseline [32] (single coil), and the end-to-end variational network (VN) [26] (PI) serve as state-of-the-art references, where the latter two primarily serve as examples of possible pitfalls in signal recovery without proper Bayesian separation. We did not include ScoreMRI in the PI experiments as it can only handle fixed-size data (320×320).

We estimate the minimum mean squared error (MMSE) by averaging ten posterior samples and, similar to [16], find the maximum a posteriori (MAP) by performing 250 accelerated gradient descent [19] steps with a fixed σ and a step size of 0.001 after the full reverse diffusion. For quantitative comparison, we calculate the peak signal-to-noise ratio (PSNR), structural similarity (SSIM), and normalized mean squared error (NMSE) with respect to the fully-samples RSS reconstruction. To quantitatively compare the reconstruction to other RSS reconstructions, we weigh the reconstruction by the RSS of the coils as described in [27], and we follow [30] and fit a spline curve to match the reconstructed and reference intensities.

4 Results

We demonstrate the interpretability of the image prior by showing the learned filters \tilde{K}_k , weights w_k , and potentials $-\log \psi_k(\cdot, w_k, t)$ for different t in Figure 1. Due to the overcompleteness of the model, the potentials significantly differ from the leptokurtic filter responses observed in [12], instead showing multiple minima different from zero, allowing the enhancement of certain image structures. This matches the observations from [3, 31, 33].

4.1 Reconstruction

Table 1 shows the quantitative results for the synthetic single coil experiment. As expected from the large, resource-intensive model, ScoreMRI [7] performs best across all sampling trajectories. The performance of the UNet, which does not follow a strictly Bayesian separation, significantly degrades for sampling trajectories different from the training setup (Cartesian with an acceleration of four). In contrast to other learning-based methods, our model has relatively few learnable parameters while achieving satisfactory results, outperforming TV across all sampling trajectories, except for the radial pattern, where it performs equally well.

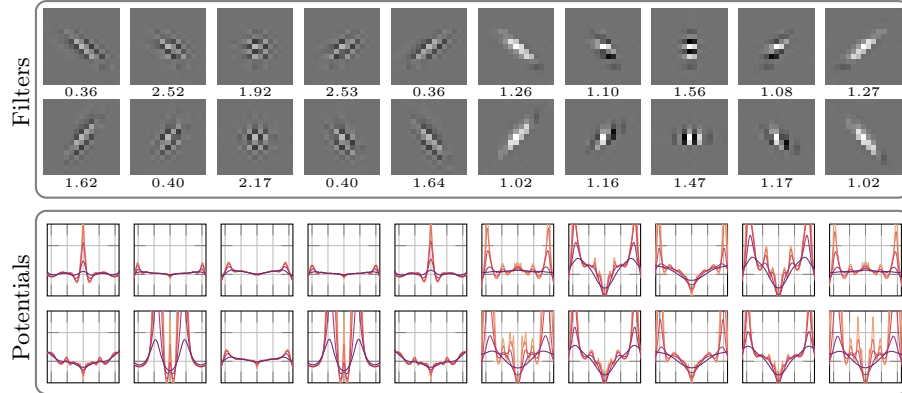


Fig. 1. The learned overcomplete model with Gaussian mixture experts. Below each filter the weight γ_k is shown. The first row shows the vertical cone and the second row is the horizontal cone of the shearlet system. The first five entries correspond to the shearing for the first scale and the second five for the second scale. The colours indicate the diffusion time $\sqrt{2t} = 0$ —, 0.025 —, 0.05 —, 0.1 —, 0.2 —.

Table 1. Quantitative results for the single-coil experiment. Bold numbers represent the best results, and underlined numbers are the second-best. The NMSE is scaled by 10^2 .

Pattern	A	Metric	ZF	TV	UNet	ScoreMRI	Ours (MMSE)
Cartesian	4	PSNR	24.03	30.2	<u>33.85</u>	34.74	31.66
		SSIM	0.69	0.81	0.87	0.87	<u>0.83</u>
		NMSE	6.32	1.23	<u>0.48</u>	0.39	0.84
Spiral	≈ 5		21.15	31.32	27.81	35.67	<u>32.99</u>
			0.63	0.84	0.78	0.88	<u>0.86</u>
			10.61	0.91	1.91	0.31	<u>0.63</u>
Radial	≈ 6		24.6	<u>31.34</u>	29.85	33.62	<u>31.34</u>
			0.68	<u>0.82</u>	0.79	0.84	<u>0.82</u>
			5.33	<u>0.89</u>	1.19	0.50	<u>0.89</u>
2D Gaussian	8		21.77	30.40	24.34	34.22	<u>33.19</u>
			0.65	<u>0.85</u>	0.73	<u>0.85</u>	0.86
			7.90	1.38	4.35	0.44	<u>0.64</u>
Learnable parameters			-	-	4.9×10^8	6.7×10^7	1578

A: Acceleration

The quantitative results for the joint nonlinear inversion in Table 2 demonstrate that our method outperforms TV on CORPD data on all sampling patterns except for Gaussian, where the performance is comparable. On CORPDFS data, our method is second to TV for most sampling trajectories, which we believe is due to the noise in the reference images, impairing quantitative comparison. This is supported by the qualitative results in Figure 4.1, where the error maps in the insets show that TV introduces significant errors in the anatomy, e.g. removing the cartilage from the tibia in the CORPDFS reconstruction, or the blood vessels in the lateral region. In contrast, our reconstruction is able to retain these features while delivering an artifact-free reconstruction. As in the single coil case, the end-to-end VN only performs well in its training configuration.

Without adding any extra computational cost to the MMSE estimate, the diffusion framework provides valuable insights into reconstruction uncertainty by delivering pixel-wise marginal variances, as shown in 4.1. Reconstructing an image of size 640×372 with 16 coils takes twenty seconds with our algorithm. In contrast, ScoreMRI [7] takes approximately five minutes to reconstruct an image of size 320×320 from single-coil data on the same hardware.

Table 2. Quantitative results for PI experiments with different sampling trajectories. The rows in each pattern alternate between PSNR, SSIM and NMSE. The NMSE is scaled by 10^2 .

Pattern	A	ACL	In-distribution (CORPD)				Out-of-distribution (CORPDFS)						
			ZF	TV	VN	Ours	ZF	TV	VN	Ours			
					MAP MMSE				MAP MMSE				
C	4	-	27.18	33.07	36.92	<u>33.22</u>	33.15	26.24	31.42	30.05	31.30	<u>31.33</u>	
			8%	0.73	0.83	0.91	<u>0.86</u>	<u>0.86</u>	0.67	0.73	0.76	<u>0.74</u>	<u>0.74</u>
				2.23	<u>0.56</u>	0.24	0.61	0.62	5.17	1.56	2.38	1.63	<u>1.61</u>
	8% ¹	31.12	33.65	24.72	35.38	<u>35.46</u>	26.52	<u>32.00</u>	28.65	32.04	31.91		
		0.81	0.83	0.67	<u>0.89</u>	0.90	0.70	0.74	0.70	0.77	<u>0.76</u>		
		0.93	<u>0.50</u>	4.01	0.33	0.33	5.09	1.40	2.91	1.40	<u>1.43</u>		
R	11	-	28.76	33.21	20.55	<u>33.63</u>	33.65	25.11	31.50	26.38	<u>31.22</u>	31.16	
			0.74	<u>0.82</u>	0.69	0.85	0.85	0.61	<u>0.72</u>	0.68	0.73	<u>0.72</u>	
			1.56	<u>0.55</u>	10.12	0.50	0.50	7.13	1.54	4.90	<u>1.65</u>	1.66	
G	8	-	32.14	34.26	23.52	<u>34.07</u>	34.00	26.66	31.99	28.20	<u>31.74</u>	31.58	
			0.83	<u>0.85</u>	0.72	0.87	0.87	0.69	<u>0.74</u>	0.71	0.75	<u>0.74</u>	
			0.73	0.43	5.20	<u>0.45</u>	0.46	5.40	1.38	3.33	<u>1.48</u>	1.52	
Learnable params.			-	-	3×10^7	1578	-	-	3×10^7	1642			

¹ horizontal; C: Cartesian, R: Radial, G: 2D Gaussian, A: Acceleration

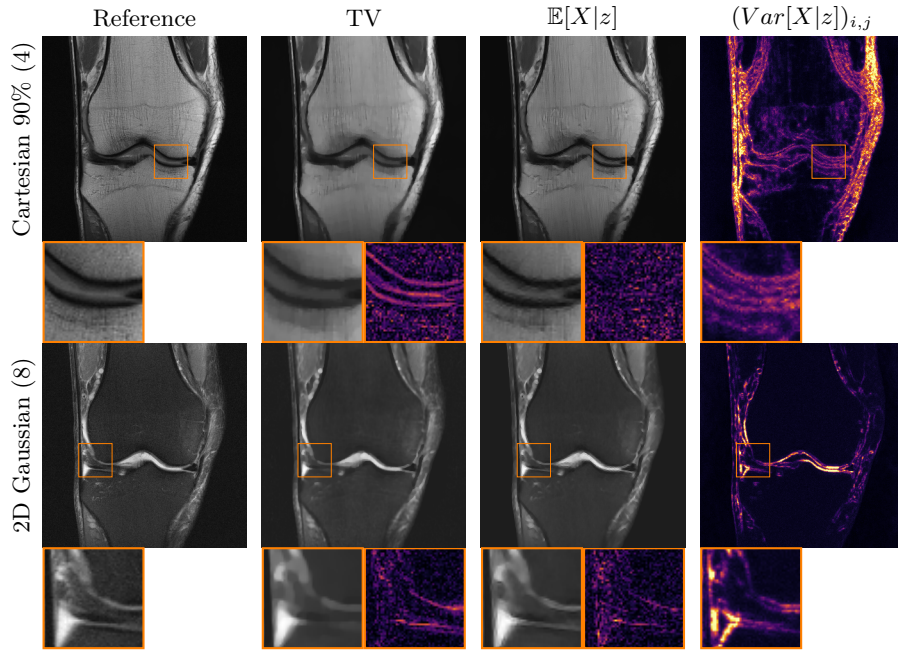



Fig. 2. Qualitative comparison for PI against TV. The first row shows results on ID data, the second on OOD data. The zoom shows an image region and the corresponding absolute error and the pixel-wise variance in the right column (0  0.25).

Finally, we compare the estimated sensitivity maps qualitatively to ESPIRiT [28] by showing the RSS null-space residuals in Figure 3, where any residual signal points to a suboptimal estimation.

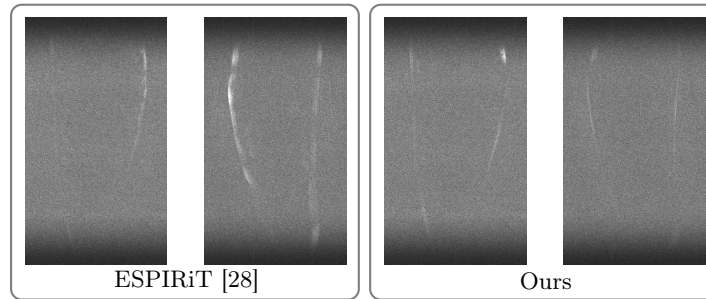


Fig. 3. RSS nullspace residuals for Cartesian subsampling. In each block, the measured data has 8% ACLs (left) and 4% ACLs (right) respectively.

We observe that [28] produces slightly better estimates than our method when more ACLs are available but falls off as the calibration region gets smaller. In contrast, our method still gives a robust estimate of the sensitivities in all cases.

5 Conclusion

In this paper, we pair an analytically tractable product of Gaussian mixture diffusion model with classic smoothness penalties to tackle the non-linear MRI reconstruction problem in the diffusion framework. The proposed method delivers satisfactory results on single- and multi-coil data, allows for fast inference, and demonstrates robustness to changes in the forward model and contrast. A drawback of the algorithm is that it requires the tuning of many hyperparameters. An interesting direction for future work includes developing a diffusion prior for $p_{X,\Sigma}$, not assuming a factorization, consequently aligning the method better with recent algorithms for posterior sampling with diffusion models.

References

1. Block, K.T., Uecker, M., Frahm, J.: Undersampled radial mri with multiple coils. iterative image reconstruction using a total variation constraint. *Magnetic Resonance in Medicine* **57**(6), 1086–1098 (2007)
2. Bogensperger, L., Chambolle, A., Pock, T.: Convergence of a piggyback-style method for the differentiation of solutions of standard saddle-point problems. *SIAM Journal on Mathematics of Data Science* **4**(3), 1003–1030 (2022)
3. Chen, Y., Pock, T.: Trainable nonlinear reaction diffusion: A flexible framework for fast and effective image restoration. *IEEE Transactions on Pattern Analysis and Machine Intelligence* **39**(6), 1256–1272 (2017)
4. Chung, H., Kim, J., Kim, S., Ye, J.C.: Parallel diffusion models of operator and image for blind inverse problems. *IEEE/CVF Conference on Computer Vision and Pattern Recognition* (2023)
5. Chung, H., Kim, J., Mccann, M.T., Klasky, M.L., Ye, J.C.: Diffusion posterior sampling for general noisy inverse problems. In: *International Conference on Learning Representations* (2023)
6. Chung, H., Sim, B., Ye, J.C.: Come-closer-diffuse-faster: Accelerating conditional diffusion models for inverse problems through stochastic contraction. *2022 IEEE/CVF Conference on Computer Vision and Pattern Recognition (CVPR)* pp. 12403–12412 (2021)
7. Chung, H., Ye, J.C.: Score-based diffusion models for accelerated mri. *Medical Image Analysis* **80**, 102479 (2022)
8. Dashti, M., Stuart, A.M.: *The Bayesian Approach to Inverse Problems*, pp. 311–428. Springer International Publishing, Cham (2017)
9. Erlacher, M., Zach, M.: Joint non-linear mri inversion with diffusion priors (2023), <https://arxiv.org/abs/2310.14842>
10. Griswold, M.A., Jakob, P.M., Heidemann, R.M., Nittka, M., Jellus, V., Wang, J., Kiefer, B., Haase, A.: Generalized autocalibrating partially parallel acquisitions (grappa). *Magnetic Resonance in Medicine* **47**(6), 1202–1210 (2002)
11. Hu, Y., Peng, A., Gan, W., Kamilov, U.S.: Adobi: Adaptive diffusion bridge for blind inverse problems with application to mri reconstruction (2024)

12. Huang, J., Mumford, D.: Statistics of natural images and models. In: Proceedings. 1999 IEEE Computer Society Conference on Computer Vision and Pattern Recognition (Cat. No PR00149). vol. 1, pp. 541–547 Vol. 1 (1999)
13. Jalal, A., Arvinte, M., Daras, G., Price, E., Dimakis, A.G., Tamir, J.: Robust compressed sensing MRI with deep generative priors. *Advances in Neural Information Processing Systems* **34**, 14938–14954 (2021)
14. Knoll, F., Bredies, K., Pock, T., Stollberger, R.: Second order total generalized variation (tgv) for mri. *Magnetic Resonance in Medicine* **65**(2), 480–491 (2011)
15. Knoll, F., Zbontar, J., Sriram, A., Muckley, M., Bruno, M., Defazio, A., Parente, M., Geras, K., Katsnelson, J., Chandarana, H., Zhang, Z., Drozdalv, M., Romero, A., Rabbat, M., Vincent, P., Pinkerton, J., Wang, D., Yakubova, N., Owens, E., Lui, Y.: fastmri: A publicly available raw k-space and dicom dataset of knee images for accelerated mr image reconstruction using machine learning. *Radiology: Artificial Intelligence* **2**, e190007 (01 2020)
16. Luo, G., Heide, M., Uecker, M.: MRI Reconstruction via Data Driven Markov Chain with Joint Uncertainty Estimation. arXiv preprint arXiv:2202.01479 (2022)
17. Lustig, M., Donoho, D., Pauly, J.M.: Sparse mri: The application of compressed sensing for rapid mr imaging. *Magnetic Resonance in Medicine* **58**(6), 1182–1195 (2007)
18. Narnhofer, D., Hammernik, K., Knoll, F., Pock, T.: Inverse gans for accelerated mri reconstruction. In: *Wavelets and Sparsity XVIII (2019)*, sPIE Optics+Photonics 2019 ; Conference date: 23-08-2019 Through 27-08-2019
19. Nesterov, Y.: A method for solving the convex programming problem with convergence rate $o(1/k^2)$. *Proceedings of the USSR Academy of Sciences* **269**, 543–547 (1983)
20. Pruessmann, K.P., Weiger, M., Scheidegger, M.B., Boesiger, P.: Sense: Sensitivity encoding for fast mri. *Magnetic Resonance in Medicine* **42**(5), 952–962 (1999)
21. Risken, H.: *The Fokker-Planck Equation: Methods of Solution and Applications*. Springer Berlin Heidelberg (1996)
22. Salimans, T., Ho, J.: Should EBMs model the energy or the score? In: *Energy Based Models Workshop - ICLR 2021* (2021)
23. Song, Y., Ermon, S.: Generative modeling by estimating gradients of the data distribution. In: *Advances in Neural Information Processing Systems*. pp. 11895–11907 (2019)
24. Song, Y., Shen, L., Xing, L., Ermon, S.: Solving inverse problems in medical imaging with score-based generative models. In: *International Conference on Learning Representations* (2022)
25. Song, Y., Sohl-Dickstein, J., Kingma, D.P., Kumar, A., Ermon, S., Poole, B.: Score-based generative modeling through stochastic differential equations. In: *International Conference on Learning Representations* (2021)
26. Sriram, A., Zbontar, J., Murrell, T., Defazio, A., Zitnick, C.L., Yakubova, N., Knoll, F., Johnson, P.: End-to-end variational networks for accelerated mri reconstruction. In: Martel, A.L., Abolmaesumi, P., Stoyanov, D., Mateus, D., Zuluaga, M.A., Zhou, S.K., Racocceanu, D., Joskowicz, L. (eds.) *Medical Image Computing and Computer Assisted Intervention – MICCAI 2020*. pp. 64–73. Springer International Publishing, Cham (2020)
27. Uecker, M., Hohage, T., Block, K.T., Frahm, J.: Image reconstruction by regularized nonlinear inversion—joint estimation of coil sensitivities and image content. *Magnetic Resonance in Medicine* **60**(3), 674–682 (2008)

28. Uecker, M., Lai, P., Murphy, M.J., Virtue, P., Elad, M., Pauly, J.M., Vasanawala, S.S., Lustig, M.: *Espirit* an eigenvalue approach to autocalibrating parallel mri: Where sense meets grappa. *Magnetic Resonance in Medicine* **71**(3), 990–1001 (2014)
29. Vincent, P.: A connection between score matching and denoising autoencoders. *Neural Computation* **23**, 1661–1674 (2011)
30. Zach, M., Knoll, F., Pock, T.: Stable deep mri reconstruction using generative priors. *IEEE transactions on medical imaging* **PP** (09 2023)
31. Zach, M., Kobler, E., Chambolle, A., Pock, T.: Product of gaussian mixture diffusion models. *Journal of Mathematical Imaging and Vision* **66**, 1–25 (03 2024)
32. Zbontar, J., Knoll, F., Sriram, A., Murrell, T., Huang, Z., Muckley, M.J., Defazio, A., Stern, R., Johnson, P., Bruno, M., Parente, M., Geras, K.J., Katsnelson, J., Chandarana, H., Zhang, Z., Drozdzal, M., Romero, A., Rabbat, M., Vincent, P., Yakubova, N., Pinkerton, J., Wang, D., Owens, E., Zitnick, C.L., Recht, M.P., Sodickson, D.K., Lui, Y.W.: *fastmri*: An open dataset and benchmarks for accelerated mri (2019)
33. Zhu, S., Mumford, D.: Prior learning and gibbs reaction-diffusion. *Pattern Analysis and Machine Intelligence, IEEE Transactions on* **19**, 1236 – 1250 (12 1997)
34. Zhuang, J., Tang, T., Ding, Y., Tatikonda, S., Dvornik, N., Papademetris, X., Duncan, J.: *Adabelief* optimizer: Adapting stepsizes by the belief in observed gradients. *Conference on Neural Information Processing Systems* (2020)